


Cite this: *Chem. Sci.*, 2025, 16, 18919 All publication charges for this article have been paid for by the Royal Society of Chemistry

# Flexible crystalline persistent fluorescence waveguides: a universal strategy for anti-counterfeiting and secure communication

Shun Liu, Linfeng Lan and Hongyu Zhang \*

The development of flexible organic crystals (FOCs) with persistent emissions represents a groundbreaking advancement in optoelectronic materials, offering transformative applications in flexible displays, secure communication, and anti-counterfeiting. Despite extensive efforts, achieving persistent emissions in FOCs remains a significant challenge, primarily due to the inherent limitations of organic molecular systems in stabilizing triplet excitons. Here, we report a universal and scalable strategy to enable long-lasting fluorescence in FOCs by incorporating a polymer coating doped with methyl-4-aminobenzoate within a poly(vinyl alcohol) matrix on crystalline substrates. Utilizing non-traditional phosphorescent radiative energy transfer mechanisms, this design transfers triplet energy of methyl-4-aminobenzoate efficiently to the FOCs, resulting in multicolor-tunable persistent fluorescence emissions. The coated FOCs demonstrate exceptional mechanical flexibility and maintain optical stability under repeated bending, while also exhibiting a robust persistent fluorescence waveguiding effect, even after UV excitation ceases. This work represents a significant breakthrough as it not only provides a solution for integrating long-lasting persistent fluorescence waveguiding properties into flexible organic systems but also enables precise modulation of optical features, laying the foundation for scalable applications in advanced encryption, anti-counterfeiting, and optoelectronic devices.

Received 7th July 2025  
Accepted 8th September 2025

DOI: 10.1039/d5sc04999g

rsc.li/chemical-science

## Introduction

Organic crystalline materials have emerged as a pivotal research frontier in materials science, owing to their exceptional optoelectronic properties, high quantum yields, and precise structural controllability.<sup>1,2</sup> These materials are widely used in optoelectronic devices such as organic light-emitting diodes (OLEDs), lasers, and sensors, benefiting from their high quantum efficiency and tunable emission properties.<sup>3–5</sup> However, the inherent rigidity of most organic crystals imposes significant limitations on their integration into flexible and dynamic optoelectronic systems, prompting researchers to explore flexible organic crystals (FOCs).<sup>6–8</sup> FOCs combine the optical advantages of organic crystals with mechanical flexibility and retain optical stability under mechanical deformation.<sup>9–12</sup> This makes FOCs highly attractive for advanced technologies, including flexible optical waveguides, dynamic information storage, and anti-counterfeiting systems.<sup>13–16</sup> To further enhance their functionality, hybridized organic crystals modified with functional coatings or molecular dopants have been developed to achieve tailored optical properties and improved stability under extreme conditions.<sup>17–19</sup>

Among these, FOCs exhibiting room-temperature phosphorescence (RTP) have attracted significant attention due to their ability to emit long-lasting luminescence from triplet states under ambient conditions.<sup>20,21</sup> Unlike fluorescence, which ceases immediately after excitation, RTP materials exhibit persistent afterglow, enabling applications in optical sensing, encrypted data storage, bioimaging, and forgery prevention.<sup>22–25</sup> Despite these advantages, achieving RTP in FOCs remains a significant challenge, primarily because of the susceptibility of triplet excitons to non-radiative decay, which severely limits emission efficiency and stability.<sup>26</sup> Conventional approaches to enhancing RTP typically involve introducing heavy atoms to increase spin–orbit coupling,<sup>27</sup> embedding organic molecules into rigid host matrices to suppress molecular motion,<sup>28,29</sup> or utilizing molecular rigidification strategies to reduce non-radiative pathways.<sup>30,31</sup> While these methods can improve triplet exciton stabilization, they are frequently constrained by synthetic complexity, reduced mechanical flexibility, and limited scalability, making them less suitable for practical applications in flexible devices. To overcome these limitations, recent research has introduced non-radiative energy transfer as a transformative strategy for achieving highly efficient and tunable RTP.<sup>32,33</sup> However, the construction of an efficient non-radiative energy transfer system is strictly constrained by distance, as energy transfer can only occur when the donor–acceptor separation is sufficiently small (10 nm for Förster

State Key Laboratory of Supramolecular Structure and Materials, College of Chemistry, Jilin University, Qianjin Street, Changchun 130012, P. R. China. E-mail: hongyuzhang@jlu.edu.cn

resonance energy transfer and 1 nm for Dexter energy transfer) and their energy levels are appropriately matched.<sup>34</sup> In contrast to non-radiative energy transfer, radiative energy transfer occurs more readily, as it is not subject to the same stringent distance constraints. Without these spatial limitations, the acceptor does not need to be co-doped with the donor but can exist as a separate luminescent layer, thereby mitigating issues related to donor-acceptor compatibility.<sup>35</sup> Moreover, integrating with polymer surface coatings can further enhance the mechanical and thermal stability of RTP materials, enabling persistent waveguiding effects under operational conditions.<sup>36–39</sup>

In this study, we propose a scalable and versatile strategy to impart persistent room-temperature fluorescence (referred to as PRTF) to flexible organic crystals through synergistic integration of phosphorescent radiative energy transfer (PRET) mechanisms with tailored polymer surface coatings. Here, PRTF refers to fluorescence emission that persists after removal of external excitation, sustained by continuous singlet-state excitation from a long-lived phosphorescent coating *via* PRET, rather than intrinsic triplet-state emission or delayed fluorescence. The polymer coatings can be used as excitation sources and support persistent fluorescence emissions from the organic crystals, even after UV excitation ceases. This approach enables the development of flexible crystals with PRTF emissions, combining delayed optical signal transmission through waveguide properties with remarkable multicolor tunability. Furthermore, by leveraging the excitation wavelength dependence of phosphorescence and fluorescence, this strategy offers the potential for dynamic optical encryption and anti-counterfeiting applications. This study establishes a novel and scalable platform for advancing flexible optoelectronic materials, bridging the gap between fundamental RTP mechanisms and practical applications. By overcoming fundamental challenges in triplet exciton stabilization and energy transfer efficiency within flexible organic crystals, this work establishes a foundation for next-generation optical encryption, data storage, and advanced anti-counterfeiting technologies.

## Results and discussion

Inspired by PRET in tunable long-lasting luminescent afterglow materials,<sup>40,41</sup> we developed a novel strategy to endow FOCs with persistent fluorescence. This strategy combines the strong fluorescence properties of organic crystals with a polymer-based coating that exhibits RTP as an excitation source, enabling long-lasting and tunable emissions. To demonstrate the versatility of this method, we synthesized crystals **1–5** previously reported<sup>42–46</sup> for their mechanically elastic bending capability and strong fluorescence ( $\lambda_{\text{em}}$ : 445–638 nm) under UV excitation (Fig. 1a). These crystals cover a broad emission wavelength range, allowing us to systematically evaluate the waveguide performance and colour characteristics of the composite materials. Importantly, the structural diversity of these crystals enables us to test the versatility of the polymer coating approach across different organic crystal surfaces, thereby confirming the general applicability of our strategy beyond a single model compound. To enable efficient PRTF, we incorporated methyl-4-

aminobenzoate (MB-NH<sub>2</sub>) doped in poly(vinyl alcohol) (PVA),<sup>47</sup> referred to as P-NH<sub>2</sub>, as the phosphor emitter (Fig. 1b). After irradiation with 254 nm, P-NH<sub>2</sub> films exhibited intense and persistent dark-blue RTP emission (Fig. S1). The hybridization process employed a layer-by-layer (LBL) self-assembly technique, wherein poly(diallyldimethylammonium chloride) (PDDA) and poly(sodium 4-styrenesulfonate) (PSS) were sequentially deposited onto the crystal surfaces.<sup>48</sup> Subsequently, the P-NH<sub>2</sub> solution was uniformly drop-cast onto the surface-modified crystals, forming a continuous and complete polymer coating (Fig. S2). The integration of P-NH<sub>2</sub> into the coating matrix effectively activates the fluorescence of the crystals, serving as a crucial component for achieving persistent afterglow emissions and tunable optical properties (Fig. 1c). After natural solvent evaporation, the hybrid crystals **1–5** (referred to as **1–5//P**) were obtained. Scanning electron microscopy (SEM) revealed that the P-NH<sub>2</sub> coating was uniformly and smoothly distributed on the crystal surfaces, with an average thickness of approximately 11.3  $\mu\text{m}$  (Fig. 1d). No observable cracks or peeling were found in the bending regions, indicating strong adhesion and mechanical integrity (Fig. 1e). Mechanical property tests revealed that the hybrid crystals retained flexibility similar to that of pristine crystals, with minimal impact on stress-strain behavior (Fig. 1f, g and S3).

The photophysical properties of P-NH<sub>2</sub> were investigated in detail under ambient conditions, revealing a broad emission band with a primary peak at 440 nm, corresponding to a dark-blue RTP emission with CIE coordinates of (0.15, 0.09) (Fig. S4). The broad RTP emission band of P-NH<sub>2</sub> is critical for enabling PRET in **1–5//P**, as the absorption spectra of crystals **1–5** significantly overlap with the emission band of P-NH<sub>2</sub> (Fig. S5).<sup>40,49</sup> This overlap facilitates efficient energy transfer from P-NH<sub>2</sub> to the crystals, thereby extending the fluorescence emission duration and enabling tunable optical performance.<sup>50</sup> Interestingly, the hybrid crystals exhibited persistent fluorescence properties that were dependent on the excitation wavelength. After 254 nm excitation, strong persistent fluorescence emissions were observed from **1–5//P** due to the robust absorption of P-NH<sub>2</sub> at this wavelength (Fig. 2a and Movie S1). In contrast, no persistent waveguide signals were detected under 365 nm excitation because of the weak absorption of the polymer coating at 365 nm (Fig. S6 and Movie S2). This phenomenon underscores the role of selective energy absorption in modulating the persistent emission behavior of the hybrid system.<sup>51</sup> In addition, the environmental stability of the material was also verified. The stability of the hybrid crystals was confirmed by monitoring their persistent fluorescence intensity, duration, and optical images under ambient laboratory conditions (254 nm excitation on 0 and 30 days). As shown in Fig. S7 and S8, the brightness and afterglow duration of **1//P** remained almost unchanged after 30 days, demonstrating excellent signal stability. This indicates that the material can maintain stable RTP performance under typical storage conditions. To further explore the PRET mechanism, we selected crystal **5** as a model system. The absorption range of crystal **5** significantly overlaps with the RTP emission of P-NH<sub>2</sub>, making it an efficient energy receptor (Fig. 2b). Under 254 nm



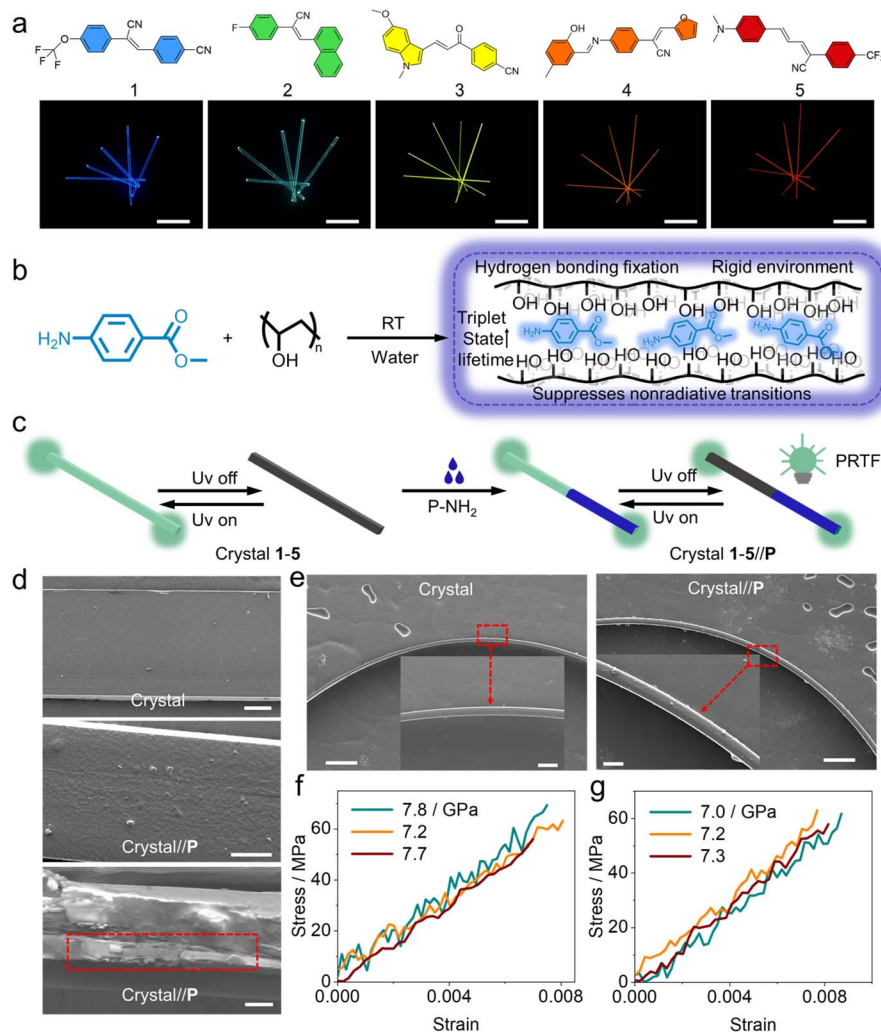


**Fig. 1** (a) Chemical structures and photographs of crystals 1–5 recorded under 365 nm UV light. (b) Synthesis strategy for dark-blue phosphorescent films (RT represents room temperature). (c) Illustration of persistent waveguide mechanisms enabled by hybridization (PRTF represents persistent room temperature fluorescence). (d) SEM images of the surface of crystal 2 (top) and surface (middle) and cross-section (bottom) of 2//P. (e) SEM images of the bent crystals 2 and 2//P. Insets show local amplification of the bending position, indicating no damage to the crystal. (f) and (g) Stress–strain curves of crystals 4 (f) and 4//P (g) obtained from three-point bending tests. The scale bars are 5 mm in panel b and 50  $\mu$ m in panels d and e.

excitation, the crystal 5 displayed a broad fluorescence emission band with a primary peak at 638 nm. When the laser was shut off, 5//P exhibited dual-emission characteristics, combining phosphorescence at 440 nm from P-NH<sub>2</sub> with fluorescence at 638 nm from crystal 5 (Fig. 2b). This spectral duality suggests an efficient energy transfer process from P-NH<sub>2</sub> to crystal 5.<sup>52,53</sup> Besides, compared to pristine crystal 5, the steady-state fluorescence intensity of 5//P remains nearly unchanged, indicating no impact from the polymer coating. After turning off excitation, the delayed persistent fluorescence intensity decreases due to indirect excitation by long-lived phosphorescence from P-NH<sub>2</sub> (Fig. S9). Lifetime measurements further corroborated this energy transfer mechanism. The fluorescence lifetime of crystal 5 at 638 nm increased significantly from 5.78 ns in its pristine state to 606.4 ms in 5//P (Fig. 2c and d). With the fluorescence lifetime of the energy acceptor (crystal 5) increases from the nanosecond to the millisecond scale, the phosphorescence

lifetime of the energy donor (P-NH<sub>2</sub>) remains nearly unchanged (Fig. S10), thereby indicating that the long-lived fluorescence originates from the excitation of P-NH<sub>2</sub> rather than the crystal itself, reflecting the long-lived emission sustained by triplet-mediated energy transfer from the P-NH<sub>2</sub> coating. This observation suggests that the energy transfer process in the composite system is primarily governed by the reabsorption mechanism, rather than Förster resonance energy transfer (FRET) or Dexter exchange energy transfer.<sup>35,40</sup> For other hybrid crystals, the phosphorescence lifetime of the polymer coating and the fluorescence lifetime of the crystal exhibit similar trends (Fig. S11, S12 and Tables S1 and S2). As illustrated in Fig. 2e, P-NH<sub>2</sub> generates RTP after laser excitation and subsequently excites the crystal *via* a radiative process. It is important to emphasize that, unlike conventional FRET systems where donor and acceptor molecules are uniformly mixed, here P-NH<sub>2</sub> is assembled as a thin film coating on the crystal surface,



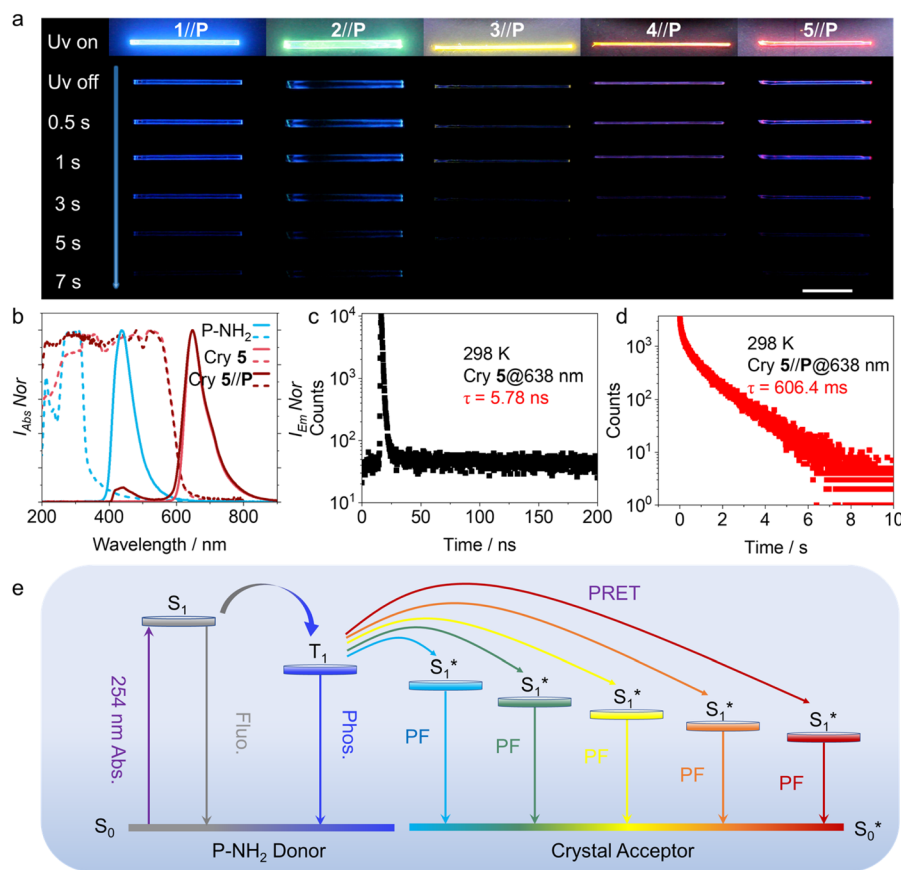


**Fig. 2** (a) Optical photographs showing persistent fluorescence of 1–5//P after 254 nm excitation. (b) Normalized UV/Vis absorption spectra (dotted lines) and emission spectra (solid lines) of P-NH<sub>2</sub>, crystal 5, and 5//P. The blue dotted and solid lines correspond to the absorption and emission spectra of P-NH<sub>2</sub>, respectively; the light red dotted and solid lines represent the absorption and emission spectra of crystal 5, respectively; and the dark red dotted and solid lines correspond to the absorption and emission spectra of 5//P, respectively. The emission spectrum of crystal 5 was recorded under continuous UV excitation. The emission spectra of P-NH<sub>2</sub> and 5//P were measured using time-gated photoluminescence with a delay time of 100 ms and gate width of 500 ms after excitation ceased. (c) and (d) Photoluminescence time-resolved decay curve of crystals 5 (c) and 5//P (d). (e) Proposed energy transfer pathway in the hybrid crystals. Phosphorescence emitted by the modified layer is absorbed by the crystal via a radiative energy transfer mechanism, resulting in persistent fluorescence emission. (PRET: phosphorescent radiative energy transfer; PF: persistent fluorescence). The scale bar in panel a is 5 mm.

resulting in physical separation exceeding 10 nm—well beyond the Förster radius. This large spatial separation precludes efficient nonradiative FRET, indicating that energy transfer predominantly occurs through radiative reabsorption (PRET).<sup>54</sup> Moreover, the RTP lifetime of P-NH<sub>2</sub> remains nearly unchanged regardless of the crystal's presence, confirming that energy transfer from P-NH<sub>2</sub> to the crystal primarily occurs *via* PRET rather than nonradiative pathways. Consequently, even after laser excitation ceases, P-NH<sub>2</sub> acts as a continuous radiative light source sustaining the crystal's persistent fluorescence emission.

Building on the persistent fluorescence and multicolour emission properties of the hybrid crystals,<sup>55,56</sup> tunable waveguide emission modes were achieved, in which 1//P and 2//P exhibited single emission signals due to significant spectral overlap between the crystal and the polymer coating (Fig. 3a and b). Specifically, 3–5//P displayed dual emission signals owing to their distinct spectral differences (Fig. 3a and c). This tunable spectral behavior further enables the realization of persistent waveguiding in hybrid crystals, expanding their functional

versatility (Fig. 3d and S13). The pristine crystals exhibited strong fluorescence under 254 nm UV irradiation, which rapidly vanished once the UV light was turned off (Fig. 3e, S13 and Movie S3). In contrast, 1–5//P demonstrated distinct and remarkable persistent waveguiding behavior under 254 nm excitation: after turning off the UV excitation source, clear waveguide signals could still be observed at the crystal tips (Fig. 3f). To verify the origin of this persistent emission, we prepared control samples coated with pure PVA (without MB-NH<sub>2</sub>). These samples exhibited prompt fluorescence under UV irradiation but showed no visible emission after the excitation was removed, confirming that the observed persistent behavior arises from the MB-NH<sub>2</sub> dopant rather than the PVA matrix itself (Fig. S14). To better understand this phenomenon, we examined the spectral data collected from both pristine and hybrid crystals during and after UV irradiation. For crystals 1–5, spectral data revealed characteristic fluorescence emission peaks under UV excitation; however, these signals rapidly decayed and vanished once the UV source was turned off (Fig. 3g). In comparison, spectral data showed that (Fig. 3h),





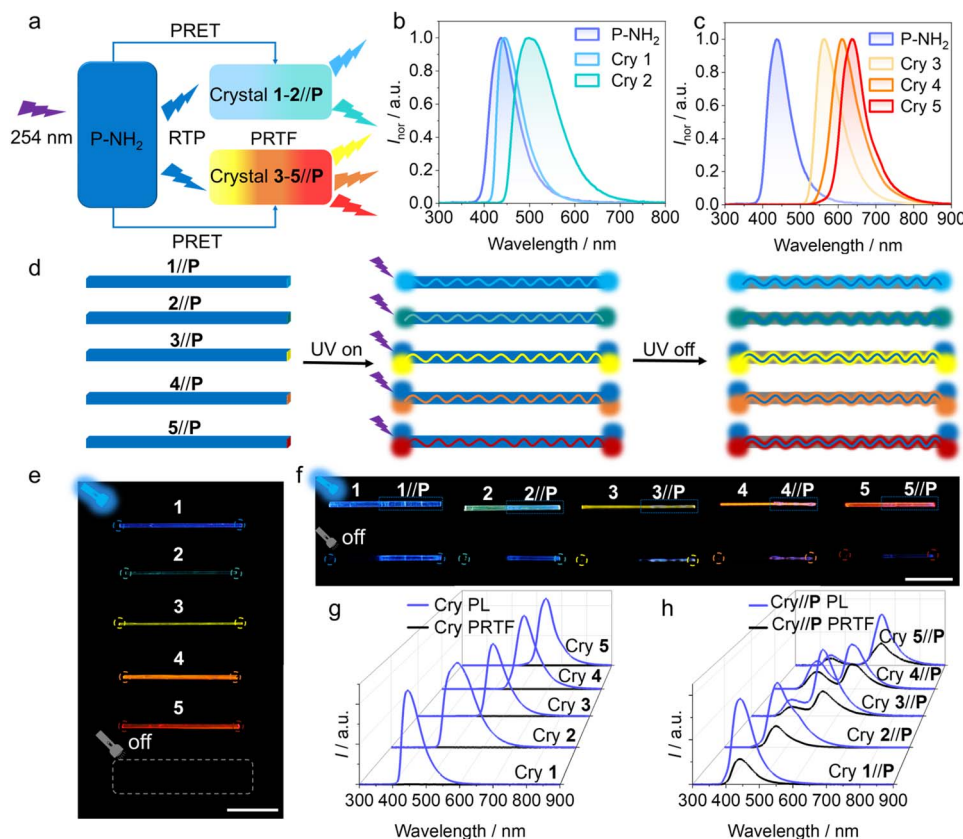


**Fig. 3** (a) Schematic representation of the different persistent fluorescence outputs of 1–5//P. (PRET: phosphorescent radiative energy transfer). (b) Normalized P-NH<sub>2</sub> phosphorescence emission spectrum and fluorescence emission spectra of crystals 1–2. (c) Normalized P-NH<sub>2</sub> phosphorescence emission spectrum and fluorescence emission spectra of crystals 3–5. (d) Schematic of persistent waveguides of 1–5//P after UV light irradiation and subsequent switching off. (e) Photographs of crystals 1–5 after UV light irradiation and switching off. (f) Photographs of partially modified 1–5//P after UV light irradiation and subsequent shutdown showing persistent waveguides (the dashed circles indicate persistent waveguides). (g) and (h) Photoluminescence (PL) spectra of crystals 1–5 (g) and 1–5//P (h) under 254 nm UV irradiation. PL was acquired under ongoing UV illumination, whereas PRTF was obtained with a 100 ms delay following cessation of the excitation. The scale bars are 5 mm.

owing to differences in the emission spectra between the polymer coating and the crystals, 1–5//P exhibited distinct emission behaviors under UV excitation: 1–2//P displayed single-peak emission, whereas 3–5//P presented dual-peak emission features. Notably, after the UV source was switched off, the spectral data of 1–5//P continued to exhibit persistent emission signals, primarily attributable to the PRET effect. This phenomenon indicates that the phosphorescence generated by the P-NH<sub>2</sub> coating acts as an energy source, which subsequently excites the crystal body to emit light. The emitted signal is then efficiently transmitted to the crystal tips through the crystal's inherent optical transducing capability, resulting in a visible waveguide output. This mechanism highlights the key role of the phosphorescent polymer layer in energy conversion and excitation, while demonstrating that the crystal core remains the main conduit for optical transmission. The pronounced waveguiding effects observed in these hybrid materials offer significant potential for applications in photonic systems, such as optical data transmission, anti-counterfeiting technologies, and programmable photonic devices. By strategically designing hybrid systems with tailored spectral properties, it is possible to

develop advanced materials for next-generation optoelectronic applications.<sup>57–60</sup>

To explore their application in flexible optical waveguides,<sup>61–63</sup> we investigated the light transmission properties of both pristine and hybrid crystals in straight and bent configurations. Under 355 nm pulsed laser excitation, emissions at one end of crystal 2 and 5 decreased with increasing distance from the excitation point, yielding optical loss coefficients (OLCs) of 0.145 and 0.148 dB mm<sup>−1</sup> for crystal 2 and 0.167 and 0.168 dB mm<sup>−1</sup> for crystal 5 in straight and bent states, respectively (Fig. S15). These low OLCs indicate that mechanical deformation has minimal impact on their optical waveguide performance.<sup>64</sup> Although the pristine crystals exhibited only conventional waveguiding capabilities, the hybrid crystals demonstrated persistent light transmission properties. Motivated by this persistent light transmission behavior, we further conducted experiments to investigate the persistent waveguiding performance. The hybrid crystals were first excited using a 254 nm UV source, and their persistent waveguiding performance was evaluated after the UV source was turned off. As shown in Fig. 4a–d and S16, after switching



off the UV source, the persistent emission intensity at one end of 2//P and 5//P gradually decreased with increasing distance from the excitation point. By fitting, the OLCs were as follows: for 2//P, 0.394 and 0.401 dB mm<sup>-1</sup> in the straight and bent states, respectively; for 5//P, the OLCs at 442 nm were 0.295 and 0.340 dB mm<sup>-1</sup> and at 640 nm they were 0.340 and 0.344 dB mm<sup>-1</sup> in the straight and bent states, respectively (Fig. S17). The experiments confirmed that the hybrid crystals are capable of maintaining persistent waveguiding behavior even after the removal of external energy input, providing an important reference for the design of novel flexible “afterglow waveguide” materials. Photographic and spectroscopic analyses revealed that the persistent waveguide effect persisted for about 7 s with stable and consistent persistent wavelengths (Fig. 4e–h and Movie S4). Since the intensity decay occurs primarily over the persistent waveguiding time rather than through spatial propagation, we replaced the distance parameter *D* with the persistent waveguiding time to characterize the temporal optical loss. For 2//P, the time decay-OLC was 1.053 dB s<sup>-1</sup>, while for 5//P, it was measured to be 1.318 dB s<sup>-1</sup> at 442 nm and 1.217 dB s<sup>-1</sup> at 640 nm (Fig. S18). Additional spectral attenuation data collected at various delay times further confirmed the reproducibility and stability of the waveguiding behavior of 2//P and 5//P (Fig. 4i–k). This exceptional persistent waveguide stability establishes hybrid crystals as promising candidates for applications in optical information transmission,<sup>65,66</sup> temporary data storage,

time-delayed communication,<sup>67,68</sup> and information security, opening new avenues for advanced photonic and optoelectronic systems.<sup>69,70</sup>

By utilizing time- and space-dependent signal outputs, we developed a robust multi-level information encryption strategy using half-coated 5//P (HC-5//P).<sup>71</sup> When the uncoated region (R-area) of HC-5//P is excited using 254 nm UV light, it produces a single red emission signal, which is defined as “1”. Upon turning off the light source, the signal vanishes instantaneously and is defined as “0” (Fig. 5a). Conversely, excitation of the coated region (B-area) generates dual emission signals at 442 nm (blue) and 640 nm (red) in both real-time and delayed modes, which are defined as “2”. By systematically exciting different positions on HC-5//P, the real-time output signals at the terminal create the first layer of encryption code, “1221212”, while the delayed signals captured after the light source is switched off form the second layer of encryption code, “0220202” (Fig. 5b and e). By modifying the excitation sequence, various delayed encryption patterns can be generated, enabling highly customizable multi-level encryption and secure information transmission (Fig. 5c, d, f and g). The application of hybrid crystals such as 1//P and 5//P in digital encryption and banknotes further demonstrates their versatility in anti-counterfeiting applications.<sup>72,73</sup> For example, the combination of hybrid and pristine crystals allows the generation of distinct cryptographic patterns under 254 nm UV excitation, with the

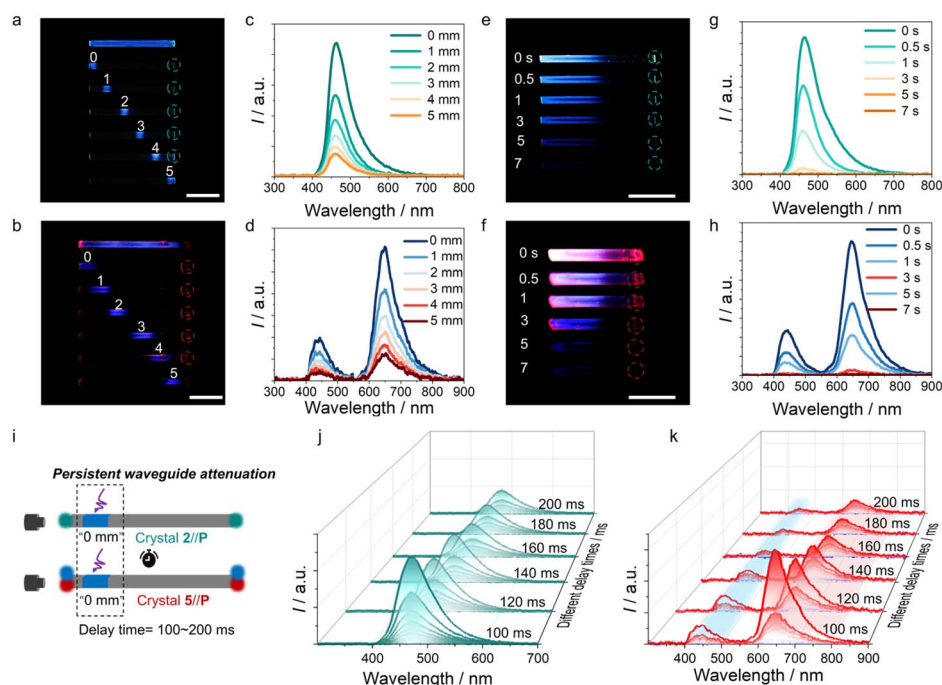


Fig. 4 (a) and (b) Persistent waveguide photographs of 2//P (a) and 5//P (b) excited with a 254 nm UV source focused at different positions in straight states, obtained 0.25 s after the UV excitation was terminated. (c) and (d) Emission spectra collected at the fixed end of 2//P and 5//P, while the crystals were excited at different positions using a 254 nm UV source. The position differences between the excitation site and the crystal terminus are defined as distance (0–5 mm), with a delay time of 100 ms. The panels c and d correspond to a and b, respectively. (e) and (f) Persistent waveguide images of 2//P (e) and 5//P (f) after 254 nm irradiation at one end. (g) and (h) Time-correlated delayed emission spectra of 2//P (g) and 5//P (h) corresponding to specific time intervals. The panels g and h correspond to e and f, respectively. (i) Schematic illustration of the waveguiding behavior of hybrid crystal at different delay times, where 5//P shows a single emission signal and 5//P exhibits dual emission signals. (j) and (k) PL spectra showing the decay of fluorescence intensity at different delay times in 2//P (j) and 5//P (k) at 0 mm. The scale bars are 5 mm.



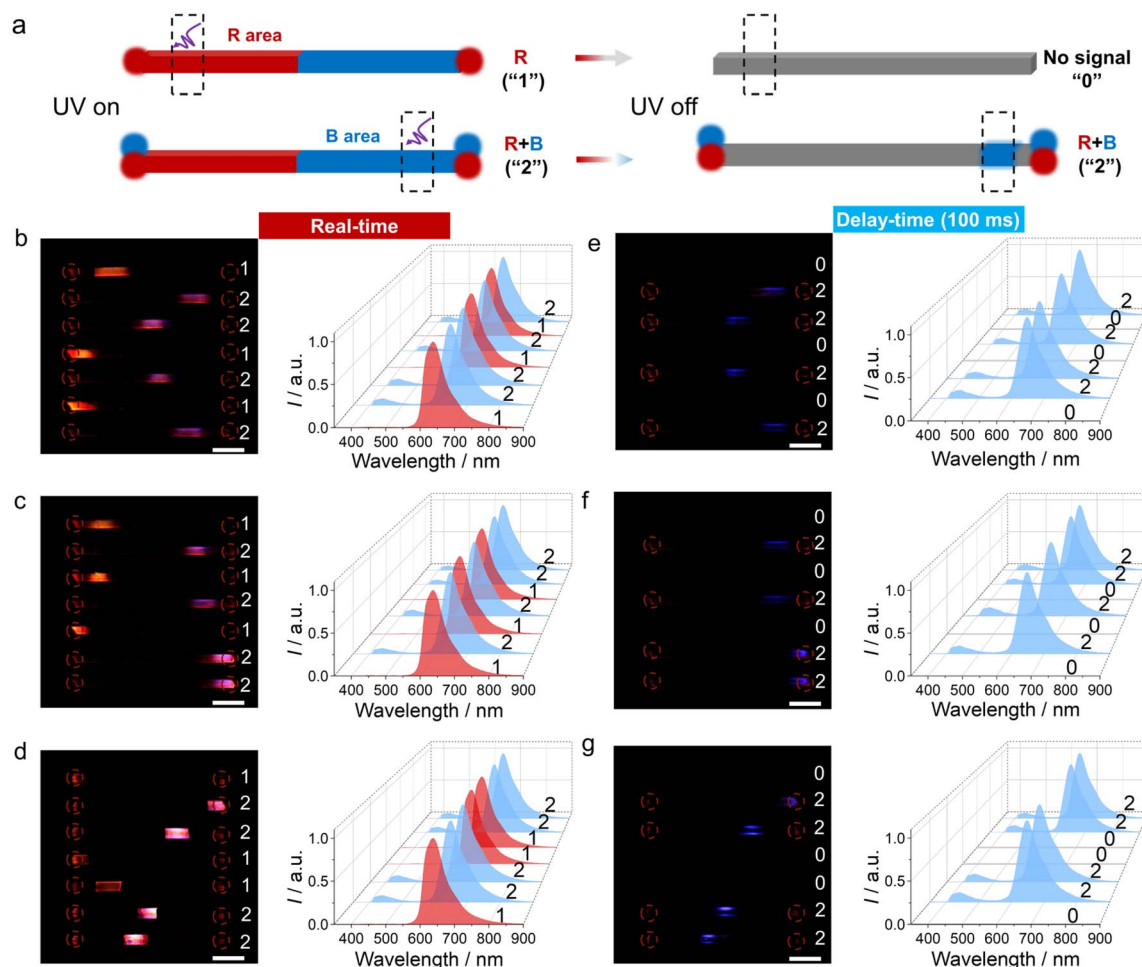


Fig. 5 (a) Schematic of signal modulation in 5//P via afterglow waveguiding after UV excitation at different positions. "0" denotes no signal output, "1" denotes single signal output, and "2" denotes dual signal output. (b)–(d) Real-time photographs and recorded spectral information of 5//P excited at different positions using a 254 nm light source. The left side shows the photographs, while the right side presents the corresponding spectra. (e)–(g) Photographs of 5//P captured 0.25 s after the shutdown of a 254 nm excitation source at different excitation positions, and the corresponding spectral data recorded with a 100 ms delay after the light source was turned off. The left side shows the photographs, while the right side presents the corresponding spectra. The scale bars are 5 mm.

persistent waveguide in the coated regions enabling a multi-layered display (Fig. S19a). 5//P demonstrates exceptional banknote security potential (Fig. S19b), combining real-time strong fluorescence with temporally persistent blue and red persistent emissions, enabling multi-level visual authentication that persists after excitation cessation. 5//P also demonstrates remarkable mechanical flexibility, maintaining both waveguide and mechanical integrity even under bending and after prolonged storage (Fig. S20). Their unique microscopic characteristics, which are challenging to replicate using conventional techniques, provide an additional level of authenticity, as they can be precisely inspected.

## Conclusions

In conclusion, this study demonstrates a hybrid strategy to achieve persistent fluorescence in FOCs, offering a universal and scalable approach to integrating room-temperature

phosphorescence and persistent fluorescence. By leveraging the synergistic effects of methyl-4-aminobenzoate doped polymer coatings and non-traditional PRET mechanisms, we have successfully enhanced the optical and mechanical properties of FOCs. The resulting materials exhibit multicolor tunable fluorescence with long-lived fluorescence and robust waveguide performance, even under mechanical deformation. Furthermore, this hybrid approach not only addresses the long-standing challenge of stabilizing triplet excitons in organic systems but also establishes a versatile framework for designing multifunctional materials. The demonstrated applications in optical encryption and advanced anti-counterfeiting highlight the transformative potential of these materials for secure communication and flexible optoelectronics. Future research should focus on further optimizing the luminescence efficiency and exploring additional hybridization strategies to expand the scope of long-afterglow materials for cutting-edge applications in sensing, displays, and high-security technologies.





## Author contributions

Shun Liu performed the experiment and data analyses and wrote the manuscript draft. Linfeng Lan revised the manuscript. Hongyu Zhang conceived the ideas, designed the research, revised the manuscript and provided funding acquisition.

## Conflicts of interest

There are no conflicts to declare.

## Data availability

All data included in this study are available upon request by contact with the corresponding author.

Supplementary information is available. See DOI: <https://doi.org/10.1039/d5sc04999g>.

## Acknowledgements

This work received support from the National Natural Science Foundation of China (52373181 and 52173164) and the Natural Science Foundation of Jilin Province (20250102120JC).

## Notes and references

- I. Divya, S. Kandasamy, S. Hasebe, T. Sasaki, H. Koshima, K. Woźniak and S. Varughese, *Chem. Sci.*, 2022, **13**, 8989–9003.
- X. Pan, L. Lan and H. Zhang, *Chem. Sci.*, 2024, **15**, 17444–17452.
- Y. Wang, L. Sun, C. Wang, F. Yang, X. Ren, X. Zhang, H. Dong and W. Hu, *Chem. Soc. Rev.*, 2019, **48**, 1492–1530.
- X. Feng, Z. Xu, Z. Hu, C. Qi, D. Luo, X. Zhao, Z. Mu, C. Redshaw, J. Lam, D. Ma and B. Tang, *J. Mater. Chem. C*, 2019, **7**, 2283–2290.
- L. Lan, L. Li, P. Naumov and H. Zhang, *Chem. Mater.*, 2023, **35**, 7363–7385.
- X. Ding, C. Wei, L. Wang, J. Yang, W. Huang, Y. Chang, C. Ou, J. Lin and W. Huang, *SmartMat*, 2024, **5**, e1213.
- J. Cao, H. Liu and H. Zhang, *CCS Chem.*, 2020, **3**, 2569–2575.
- J. Zhu, W. Wu, H. Qi, Y. Yao, H. Yu, X. Huang, N. Wang, T. Wang and H. Hao, *Chem. Sci.*, 2024, **15**, 18617–18626.
- J. Lin, J. Zhou, Z. Wang, L. Li, M. Li, J. Xu, S. Wu, P. Naumov and J. Gong, *Angew. Chem., Int. Ed.*, 2024, **64**, e202416856.
- B. Tang, B. Liu, H. Liu and H. Zhang, *Adv. Funct. Mater.*, 2020, **30**, 2004116.
- B. Tang, X. Yu, K. Ye and H. Zhang, *Adv. Opt. Mater.*, 2022, **10**, 2101335.
- R. Chinnasamy, J. Ravi, V. Vinay Pradeep, D. Manoharan, F. Emmerling, B. Bhattacharya, S. Ghosh and R. Chandrasekar, *Chem.–Eur. J.*, 2022, **28**, e202200905.
- G. Yang, H. Xin, Z. Liang, Y. Zhang, L. Wang, Z. Cheng, S. Zhao, Z. Liu and D. Cao, *Adv. Opt. Mater.*, 2025, **13**, 2401922.
- L. Lan, X. Pan, P. Commins, L. Li, L. Catalano, D. Yan, H. Xiong, C. Wang, P. Naumov and H. Zhang, *CCS Chem.*, 2025, **7**, 905–917.
- W. Wu, K. Chen, T. Wang, N. Wang, X. Huang, L. Zhou, Z. Wang and H. Hao, *J. Mater. Chem. C*, 2023, **11**, 2026–2052.
- M. Liang, S. Hu, Y. Han, Z. Liu, C. Li, J. Hao and P. Xue, *ACS Appl. Mater. Interfaces*, 2023, **15**, 37855–37866.
- L. Lan, H. Liu, X. Yu, X. Liu and H. Zhang, *Angew. Chem., Int. Ed.*, 2021, **60**, 11283–11287.
- D. Muleta, J. Song, W. Feng, R. Wu, X. Zhou, W. Li, L. Wang, D. Liu, T. Wang and W. Hu, *J. Mater. Chem. C*, 2021, **9**, 5093–5097.
- X. Yang, L. Lan, X. Pan, X. Liu, Y. Song, X. Yang, Q. Dong, L. Li, P. Naumov and H. Zhang, *Nat. Commun.*, 2022, **13**, 7874.
- Y. Xia, C. Zhu, F. Cao, Y. Shen, M. Ouyang and Y. Zhang, *Angew. Chem., Int. Ed.*, 2023, **62**, e202217547.
- H. Liu, Z. Bian, Q. Cheng, L. Lan, Y. Wang and H. Zhang, *Chem. Sci.*, 2019, **10**, 227–232.
- Q. Zhou, M. Feng, C. Shi, M. Qian, X. Ma, R. He, X. Meng, Y. Shi, Q. Cao and L. Zheng, *Chem. Sci.*, 2025, **16**, 9988–9997.
- D. Ma, Z. Li, K. Tang, Z. Gong, J. Shao and Y. Zhong, *Nat. Commun.*, 2024, **15**, 4402.
- K. Wan, Y. Zhai, S. Liu, J. Li, S. Li, B. Strehmel, Z. Chen and T. James, *Angew. Chem., Int. Ed.*, 2022, **61**, e202202760.
- Y. Zhang, H. Li, M. Yang, W. Dai, J. Shi, B. Tong, Z. Cai, Z. Wang, Y. Dong and X. Yu, *Chem. Commun.*, 2023, **59**, 5329–5342.
- J. Cui, S. Ali, Z. Shen, W. Xu, J. Liu, P. Li, Y. Li, L. Chen and B. Wang, *Chem. Sci.*, 2024, **15**, 4171–4178.
- W. Dai, Y. Jiang, Y. Lei, X. Huang, P. Sun, J. Shi, B. Tong, D. Yan, Z. Cai and Y. Dong, *Chem. Sci.*, 2024, **15**, 4222–4237.
- H. Sun, R. Ding, S. Lv, S. Zhou, S. Guo, Z. Qian and H. Feng, *J. Phys. Chem. Lett.*, 2020, **11**, 4962–4969.
- Y. Gao, J. Wang, C. Sun and T. Su, *Chem. Phys.*, 2023, **573**, 112006.
- T. Wang, M. Liu, J. Mao, Y. Liang, L. Wang, D. Liu, T. Wang and W. Hu, *Chin. Chem. Lett.*, 2024, **35**, 108385.
- L. Liang, B. Chen, Y. Gao, J. Lv, M. Liu and D. Li, *Adv. Mater.*, 2024, **36**, 2308180.
- S. Kuila and S. George, *Angew. Chem., Int. Ed.*, 2020, **59**, 9393–9397.
- Y. Ma, H. Xiao, X. Yang, L. Niu, L. Wu, C. Tung, Y. Chen and Q. Yang, *J. Phys. Chem. C*, 2016, **120**, 16507–16515.
- H. Liu, J. Chen, Y. Fu, Z. Zhao and B. Tang, *Adv. Funct. Mater.*, 2021, **31**, 2103273.
- J. Chen, Z. Xie, Y. Shan, T. Wang and B. Liu, *Adv. Opt. Mater.*, 2024, **12**, 2302458.
- H. Yao, F. Yang, J. Hu, W. Cao, S. Qin, T. Wei, B. Shi and Q. Li, *Chin. Chem. Lett.*, 2024, 110375.
- Z. Li, L. Liao, S. Liu, Y. Mu, Y. Huo and F. Liang, *J. Lumin.*, 2023, **263**, 119978.
- F. Wang, Y. Wang, R. Guo, Y. Wu, S. Zhou, H. Xiao and X. Sun, *Chem. Commun.*, 2024, **60**, 5419–5422.
- K. Hayashi, K. Fukasawa, T. Yamashita and S. Hirata, *Chem. Mater.*, 2022, **34**, 1627–1637.





- 40 L. Ma, Q. Xu, S. Sun, B. Ding, Z. Huang, X. Ma and H. Tian, *Angew. Chem., Int. Ed.*, 2022, **61**, e202115748.
- 41 K. Cheng, Z. Guo, P. Zhang, L. Feng, Y. Zhou, L. Li, H. Song, T. Wang, Y. Zhao and L. Zhao, *Laser Photonics Rev.*, 2025, **19**, 2401524.
- 42 L. Lan, L. Li, C. Wang, P. Naumov and H. Zhang, *J. Am. Chem. Soc.*, 2024, **146**, 30529–30538.
- 43 X. Yang, L. Lan, L. Li, J. Yu, X. Liu, Y. Tao, Q. Yang, P. Naumov and H. Zhang, *Nat. Commun.*, 2023, **14**, 3627.
- 44 Q. Di, J. Li, Z. Zhang, X. Yu, B. Tang, H. Zhang and H. Zhang, *Chem. Sci.*, 2021, **12**, 15423–15428.
- 45 L. Lan, X. Yang, B. Tang, X. Yu, X. Liu, L. Li, P. Naumov and H. Zhang, *Angew. Chem., Int. Ed.*, 2022, **61**, e202200196.
- 46 Q. Chen, B. Tang, K. Ye and H. Zhang, *Adv. Mater.*, 2024, **36**, 2311762.
- 47 L. Zhou, J. Song, Z. He, Y. Liu, P. Jiang, T. Li and X. Ma, *Angew. Chem., Int. Ed.*, 2024, **63**, e202403773.
- 48 X. Yang, L. Lan, I. Tahir, Z. Alhaddad, Q. Di, L. Li, B. Tang, P. Naumov and H. Zhang, *Nat. Commun.*, 2024, **15**, 9025.
- 49 P. Liao, T. Wu, C. Ma, J. Huang and Y. Yan, *Adv. Opt. Mater.*, 2023, **11**, 2202482.
- 50 D. Wang, J. Gong, Y. Xiong, H. Wu, Z. Zhao, D. Wang and B. Tang, *Adv. Funct. Mater.*, 2023, **33**, 2208895.
- 51 Z. Wang, Y. Zhang, C. Wang, X. Zheng, Y. Zheng, L. Gao, C. Yang, Y. Li, L. Qu and Y. Zhao, *Adv. Mater.*, 2020, **32**, 1907355.
- 52 K. Chen, Y. Xiong, D. Wang, Y. Pan, Z. Zhao, D. Wang and B. Tang, *Adv. Funct. Mater.*, 2024, **34**, 2312883.
- 53 T. Kwon, M. Kim, J. Kwon, D. Shin, S. Park, C. Lee, J. Kim and J. Hong, *Chem. Mater.*, 2007, **19**, 3673–3680.
- 54 R. Deng, J. Wang, R. Chen, W. Huang and X. Liu, *J. Am. Chem. Soc.*, 2016, **138**, 15972–15979.
- 55 S. Liu, Y. Lin and D. Yan, *Sci. China: Chem.*, 2023, **66**, 3532–3538.
- 56 S. Li, J. Gu, J. Wang, W. Yuan, G. Ye, L. Yuan, Q. Liao, L. Wang, Z. Li and Q. Li, *Adv. Sci.*, 2024, **11**, 2402846.
- 57 Q. Di, M. Al-Handawi, L. Li, P. Naumov and H. Zhang, *Angew. Chem., Int. Ed.*, 2024, **63**, e202403914.
- 58 L. Lan, L. Li, J. Qi, X. Pan, Q. Di, P. Naumov and H. Zhang, *Nat. Commun.*, 2023, **14**, 7582.
- 59 X. Yang, M. Al-Handawi, L. Li, P. Naumov and H. Zhang, *Chem. Sci.*, 2024, **15**, 2684–2696.
- 60 B. Tang, S. Tang, C. Qu, K. Ye, Z. Zhang and H. Zhang, *CCS Chem.*, 2023, **5**, 2348–2357.
- 61 T. Ji, X. Yang, Q. Chen and H. Zhang, *Chem. Sci.*, 2025, **16**, 8099–8107.
- 62 L. Lan and H. Zhang, *Angew. Chem., Int. Ed.*, 2024, **63**, e202411405.
- 63 H. Liu, Z. Lu, Z. Zhang, Y. Wang and H. Zhang, *Angew. Chem., Int. Ed.*, 2018, **57**, 8448–8452.
- 64 M. Dai, Z. Qi and D. Yan, *Angew. Chem., Int. Ed.*, 2025, **64**, e202420139.
- 65 C. Huang, Y. Zhang, J. Zhou, S. Sun, W. Luo, W. He, J. Wang, X. Shi and M. Fung, *Adv. Opt. Mater.*, 2020, **8**, 2000727.
- 66 S. Song, T. Hao, B. Wang, D. Liu, Z. Ren, Y. Zhang, W. Liu, L. Zhang and Y. Li, *Adv. Opt. Mater.*, 2023, **11**, 2301065.
- 67 X. Pan, L. Lan, L. Li, P. Naumov and H. Zhang, *Angew. Chem., Int. Ed.*, 2024, **63**, e202320173.
- 68 H. Chen, N. Cheng, W. Ma, M. Li, S. Hu, L. Gu, S. Meng and X. Guo, *ACS Nano*, 2016, **10**, 436–445.
- 69 C. Xing, Z. Qi, Y. Ma, D. Yan and W. Fang, *Angew. Chem., Int. Ed.*, 2025, **64**, e202502782.
- 70 M. Dai, B. Zhou and D. Yan, *Angew. Chem., Int. Ed.*, 2025, **64**, e202505322.
- 71 A. Cui, X. Miao, J. Yue, X. Sun, Q. Yu, D. Zhang, T. Zhang, T. Fei and C. Chen, *Adv. Funct. Mater.*, 2024, **34**, 2401880.
- 72 K. Huang, L. Song, K. Liu, A. Lv, M. Singh, K. Shen, J. Shen, J. Wang, H. Wang, H. Shi, H. Ma, M. Gu, G. Sun, W. Yao, Z. An and W. Huang, *npj Flexible Electron.*, 2021, **5**, 21.
- 73 P. Samadder, K. Naim, S. Sahoo and P. Neelakandan, *Chem. Sci.*, 2024, **15**, 9258–9265.

